# Brownian motion of solitons in a Bose–Einstein condensate

**Lauren M. Aycock[a,b], Hilary M. Hurst[a,c], Dmitry K. Efimkin[d], Dina Genkina[a], Hsin-I Lu[a], Victor M. Galitski[a,c], and I. B. Spielman[a,1]**

[a]Joint Quantum Institute, National Institute of Standards and Technology and University of Maryland, Gaithersburg, MD, 20899; [b]Department of Physics, Cornell University, Ithaca, NY 14850; [c]Condensed Matter Theory Center, Department of Physics, University of Maryland, College Park, MD 20742; and [d]The Center for Complex Quantum Systems, The University of Texas at Austin, Austin, TX 78712-1192

Edited by Alain Aspect, Institut d'Optique, Palaiseau, France, and approved January 10, 2017 (received for review September 7, 2016)

**We observed and controlled the Brownian motion of solitons. We launched solitonic excitations in highly elongated $^{87}$Rb Bose–Einstein condensates (BECs) and showed that a dilute background of impurity atoms in a different internal state dramatically affects the soliton. With no impurities and in one dimension (1D), these solitons would have an infinite lifetime, a consequence of integrability. In our experiment, the added impurities scatter off the much larger soliton, contributing to its Brownian motion and decreasing its lifetime. We describe the soliton's diffusive behavior using a quasi-1D scattering theory of impurity atoms interacting with a soliton, giving diffusion coefficients consistent with experiment.**

soliton | Brownian motion | Bose–Einstein condensate | diffusion | fluctuation dissipation

We studied the diffusion and decay of solitons in the highly controlled quantum environment provided by atomic Bose–Einstein condensates (BECs), where density maxima can be stabilized by attractive interactions [i.e., bright solitons (1, 2)] or, as here, where density depletions can be stabilized by repulsive interactions [i.e., dark solitons such as kink solitons (3, 4) and solitonic vortices (5)]. By contaminating these BECs with small concentrations of impurity atoms, we quantitatively studied how random processes destabilize solitons.

Our BECs can be modeled by the one-dimensional (1D) Gross–Pitaevski equation (GPE): an integrable nonlinear wave equation with soliton solutions as excitations above the ground state. For a homogeneous 1D BEC of particles with mass $m_{\mathrm{Rb}}$ with density $\rho_0$, speed of sound $c$, and healing length $\xi = \hbar/\sqrt{2}m_{\mathrm{Rb}}c$, the dark soliton solutions

$$\varphi(z,t) = \sqrt{\rho_0}\left[i\frac{v_s}{c} + \frac{\xi}{\xi_s}\tanh\left(\frac{z - v_s t}{\sqrt{2}\xi_s}\right)\right] \qquad [1]$$

are expressed in terms of time $t$, axial position $z$, soliton velocity $v_s$, and soliton width $\xi_s = \xi/\sqrt{1-(v_s/c)^2}$. Such dark solitons have a minimum density $\rho_0(v_s/c)^2$ and a phase jump $-2\cos^{-1}(v_s/c)$, both dependent on the soliton velocity $v_s$. These behave as classical objects with a negative inertial mass $m_s \approx -4\hbar\rho_0/c$, essentially the missing mass of the displaced atoms. The negative mass implies that increasing the soliton velocity reduces its kinetic energy; thus, dissipation accelerates dark solitons (6). This can be seen from the soliton equation of motion

$$-|m_s|\ddot{z}(t) = -\gamma\dot{z}(t) - \partial_z V + f(t), \qquad [2]$$

where $-\gamma\dot{z}$ is the friction force and $V$ is the confining potential due to the mean-field effects of the condensate. The random Langevin force $f(t)$ has a white noise correlator $\langle f(t)f(t')\rangle = 2\gamma k_{\mathrm{B}}T\delta(t-t')$, where $T$ is temperature and $k_{\mathrm{B}}$ is Boltzmann's constant. The connection between the friction coefficient $\gamma$ and $f(t)$ derives from the same microscopic dynamics that yield the fluctuation–dissipation theorem for positive mass objects—$f(t)$ is responsible for Brownian motion, whereas $\gamma$ describes friction, but both have contributions from impurity atoms.

Conventionally, the diffusion coefficient $D$ is inversely proportional to the friction coefficient: $D \propto 1/\gamma$. For negative mass objects, we show that the diffusion coefficient is instead proportional to the friction coefficient $D \propto \gamma$; this reflects that friction is an antidamping force for negative mass objects. The interplay between friction and confinement drives diffusive behavior with linear-in-time variance in soliton position, $\mathrm{Var}(z) = Dt$, the same Brownian motion present for positive mass objects.

Solitons are infinitely long lived because of the integrability of the 1D GPE. Integrability breaking is inherent in all physical systems—for example, from the nonzero transverse extent of quasi-1D systems. Indeed, the kink soliton in 3D—the direct analogue to the 1D GPE's dark soliton solution—is only long-lived in highly elongated geometries (7–9), where integrability breaking is weak. Cold atom experiments have profoundly advanced our understanding of soliton instability by controllably lifting integrability by tuning the dimensionality (5, 10). Here, we studied the further lifting of integrability by coupling solitons to a reservoir of impurities.

## Experimental System

Our system (11) consisted of an elongated $^{87}$Rb BEC, confined in a nominally flat-bottomed time-averaged potential, created by spatially dithering one beam of our crossed dipole trap. We

### Significance

**Solitons, spatially localized, mobile excitations resulting from an interplay between nonlinearity and dispersion, are ubiquitous in physical systems from water channels and oceans to optical fibers and Bose–Einstein condensates (BECs). From our pulse throbbing at our wrists to rapidly moving tsunamis, solitons appear naturally at a wide range of scales. In nonlinear optical fibers, solitons can travel long distances with applications for communication technology and potential for use in quantum switches and logic. Understanding how random processes contribute to the decay and the diffusion of solitons is essential to advancing these technologies.**

PHYSICS

Author contributions: V.M.G. and I.B.S. designed research; V.M.G. proposed the initial theoretical concept that I.B.S. refined into a working experimental concept; H.M.H., D.K.E., and V.M.G. developed the final theoretical framework; L.M.A. configured the apparatus for this experiment; L.M.A led the data acquisition and analysis effort to which D.G. and H.-I.L. contributed; H.M.H. performed detailed simulations for our experiment; I.B.S. contributed to the understanding of experimental data; H.M.H. prepared the theory discussions in the manuscript; and L.M.A., H.M.H., D.G., H.-I.L., V.M.G., and I.B.S. wrote the paper.

The authors declare no conflict of interest.

This article is a PNAS Direct Submission.

[1]To whom correspondence should be addressed. Email: ian.spielman@nist.gov.

prepared $N = 8(2) \times 10^5$ atoms* in the $|F=1, m_F=0\rangle$ internal state at $T = 10(5)$ nK. Our system's $\approx 250\,\mu$m longitudinal extent was approximately 30 times its transverse Thomas–Fermi diameter $2R_\perp$ set by the radial trap frequency $\omega_r = 2\pi \times 115(2)$ Hz and chemical potential $\mu \approx h \times 1$ kHz. We controllably introduced a uniform (12) gas of $N_I$ impurity atoms in thermal equilibrium, with our BECs using an rf pulse resonant with the $|F=1, m_F=0\rangle$ to $|F=1, m_F=+1\rangle$ transition before evaporation to degeneracy (13). This gave impurity fractions $N_I/N$ from 0 to 0.062 in our final BECs.

We then launched long-lived solitonic excitations using a phase-imprinting technique (3, 4. Because our trap geometry had a finite transverse extent, quantified by the ratio $\mu/\hbar\omega_r \approx 9$, planar kink solitons could be dynamically unstable and decay into 3D excitations (14). Our soliton's initial velocity $v_s \approx 0.3$ mm/s, approximately $1/5$ the 1D speed of sound $c \approx 1.4$ mm/s (15), implies that it is in an unstable regime (6), where it will convert from a planar kink soliton to a nearly planar solitonic vortex. For highly anisotropic geometries such as ours, the density profile of these two types of solitons is nearly the same—as given by the 1D GPE—reflecting that they become formally indistinguishable at large velocity (14).

We absorption-imaged our solitons after a sufficiently long time-of-flight (TOF) that their initial width $\xi_s \approx 0.24\,\mu$m expanded beyond our $\approx 2\,\mu$m imaging resolution. Fig. 1*A* shows our elongated BEC with no soliton present, and, in contrast, Fig. 1*B* displays a BEC with a soliton taken 0.947 s after its inception. The soliton is the easily identified density depletion sandwiched between two density enhancements. We quantitatively identified the soliton position as the minimum of the density depletion from 1D distributions (Fig. 1 *B*, *Right*). Our phase-imprinting process launched several excitations in addition to the soliton of interest. After a few hundred milliseconds, the additional excitations dissipated, and the remaining soliton was identified. By backtracking the soliton trajectory, we were able to identify the soliton, even at short times.

Fig. 1*E* shows a series of 1D distributions taken from time $t \approx 0$ s to 4 s after the phase imprint. These images show three salient features: (*i*) The soliton underwent approximately sinusoidal oscillations; (*ii*) the soliton was often absent at long times; and (*iii*) there was significant scatter in the soliton position. Items *ii* and *iii* suggest that random processes were important to the soliton's behavior. The solitons' position $z_i$—when present—is represented by the light pink symbols in Fig. 1*D*, and the darker pink symbols mark the average position $\langle z_i \rangle$ for each time $t$.

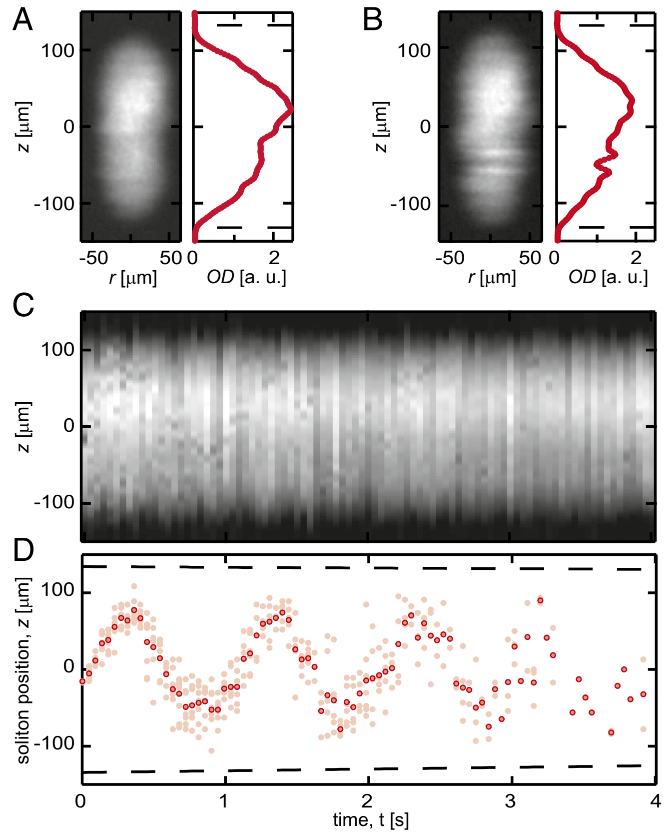


**Fig. 1.** Soliton oscillations. (*A*) An absorption image after a 19.3 ms TOF of an elongated condensate without a soliton and a longitudinal density distribution obtained by averaging over the remaining transverse direction. (*B*) An absorption image and 1D distribution at time $t = 0.942$ s with a soliton with $\approx$30% imaged contrast. (*C*) A subset of the data where each 1D distribution is a unique realization of the experiment plotted vs. time $t$. Notice a soliton was often absent at longer times. (*D*) The axial position $z_i$ of the soliton (light pink) vs. time $t$ for different realizations of the experiment. We repeated each measurement 8 times. Dashed lines represent the edges of the elongated condensate. The dark markers represent the average soliton position $\langle z_i \rangle$ at each time $t$. In *A* and *B* the longitudinal densities are given in arbitrary units (a.u.).

## Coupling to Impurities

Having established a procedure for creating solitons, we turned to the impact of coupling to a reservoir of impurities, thus further breaking integrability. Fig. 2 displays the soliton position vs. time for a range of impurity fractions. Adding impurities gave two dominant effects†: further increasing the scatter in the soliton position $z$ and further decreasing the soliton lifetime. These effects manifested as a reduced fraction $f_s$ of images with a soliton present and an increase in the sample variance $\mathrm{Var}(z) = \sum (z_i - \langle z \rangle)^2/(M-1)$ computed by using the number $M$ of measured positions $z_i$ at each time.

**Reduced Lifetime.** The addition of impurities had a dramatic impact on the soliton lifetime. Although we lack a quantitative model of the soliton's decay mechanism, there are several reasons to expect a finite lifetime. When dissipation is present, solitons accelerate to the speed of sound and disintegrate. Furthermore, numerical simulations show that, in anharmonic traps, solitons lose energy by phonon emission, accelerate, and ultimately decay (16). All of these decay mechanisms can contribute to the soliton lifetime, even absent impurities.

The added impurities act as scatterers impinging on the soliton, further destabilizing it. This effect is captured in Fig. 3*A*, showing the measured survival probability $f_s$ vs. time for a range of impurity fractions. We fit to our data a model of the survival probability

$$f_s(t) = 1 - \frac{1}{2}\,\mathrm{erfc}\left[\frac{-\ln(t/\tau)}{\sqrt{2}\sigma}\right], \quad [3]$$

essentially the integrated lognormal distribution of decay times, suitable for decay due to accumulated random processes (17). The survival probability $f_s(t)$ has a characteristic width parameterized by $\sigma$ and reaches $1/2$ at time $\tau$, which we associate with the soliton lifetime. Fig. 3*B* shows the extracted lifetime $\tau$ vs. impurity fraction $N_I/N$, showing a monotonic decrease. Our maximum $N_I/N$ gives a factor of four decrease in lifetime $\tau$.

*In our system, number fluctuations increased at the lowest trap depth (*Materials and Methods*).

†The soliton oscillation frequency was slightly shifted with impurities resulting from an unintentional change in the underlying optical potential. This change also slightly reduced the BECs' longitudinal extent.

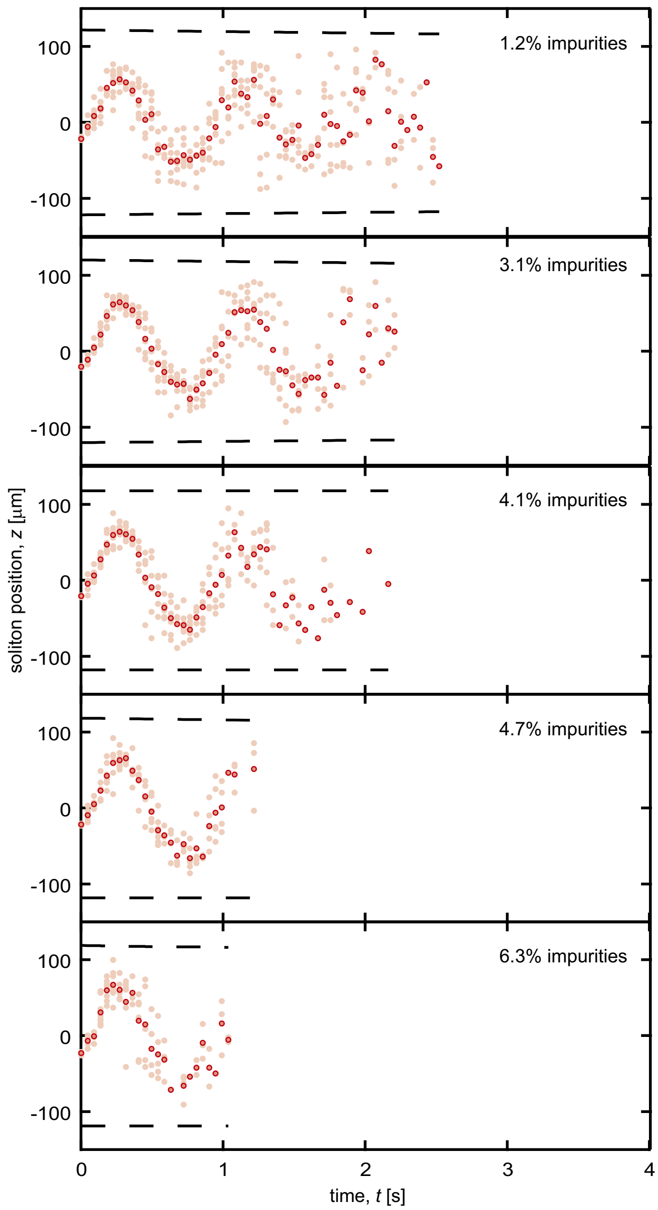


**Fig. 2.** Impact of impurities. Here, we plot the position $z_i$ of the soliton (light pink) vs. time $t$ after the phase imprint for different impurity levels. The dark pink markers represent the average position $\langle z_i \rangle$ for each time $t$. Dashed lines represent the endpoints of the condensate vs. $t$.

**Soliton Diffusion.** The second important consequence of adding impurities was an increased scatter in soliton position $z$, reminiscent of Brownian motion. Indeed, as shown in Fig. 4*B*, this scatter, quantified by $\mathrm{Var}(z)$, increased linearly with time. We obtained the diffusion coefficient $D$ as the slope from linear fits to these data and calculated $D$ using a quasi-1D scattering theory. The energy of the infinitely long 1D system is given by the GPE energy functional

$$E\left[\varphi, \psi\right] = \int \left( \frac{\hbar^2 |\nabla\varphi|^2}{2m_{\mathrm{Rb}}} + \frac{\hbar^2 |\nabla\psi|^2}{2m_{\mathrm{Rb}}} + \frac{g}{2}|\varphi|^2|\varphi|^2 + \frac{g'}{2}|\varphi|^2|\psi|^2 \right) dz, \quad \textbf{[4]}$$

describing the majority gas interacting with itself along with the impurities with interaction coefficients $g$ and $g'$, respectively. The fields $\varphi$ and $\psi$ denote the condensate and impurity wave functions. Because the impurities are very dilute, we do not include interactions between impurity atoms. A soliton (Eq. **1**) acts as a supersymmetric Pöschl–Teller (18, 19) potential for the impurity atoms with exact solutions in terms of hypergeometric functions (20). Impurity scattering states with momentum $k_z$ in the rest frame of the soliton are described by the reflection coefficient

$$R(k_z) = \frac{1 - \cos(2\pi\lambda)}{\cosh(2\pi k_z \xi) - \cos(2\pi\lambda)}, \quad \textbf{[5]}$$

where $\lambda(\lambda - 1) = g'/g$. In $^{87}$Rb, we have $g \approx g'$, giving $\lambda \approx 1.5$. The scattering problem is fully characterized by $R(k_z)$, and the problem is reduced to that of a classical heavy object moving through a gas of lighter particles.

To understand soliton diffusion over many experimental runs, we studied their distribution function $f(t, z, v_s)$. We used a kinetic equation equivalent to Eq. **2** with a stochastic force due to elastic collisions with the impurity atoms and a harmonic confining potential $V(z) \approx -|m_s|\omega^2 x^2/2$, where $\omega = \omega_{\mathrm{trap}}/\sqrt{2}$ is the effective frequency (21, 22). In the limit of small soliton velocity $(v_s/c)^2 \ll 1$, the time-dependent distribution function can be calculated exactly (*Materials and Methods*). The kinetic equation has no stable solutions: Eventually, all solitons accelerate and disappear. However, the timescale for acceleration is set by $\Gamma^{-1} = |m_s|/\gamma$, was many seconds in our experiment. In the limit of $\Gamma t \ll 1$ and $\Gamma \ll \omega$, the variance in position grew linearly with time and diffusive behavior emerges (i.e., $\mathrm{Var}(z) \approx Dt$). We calculate the diffusion coefficient

$$D \approx \frac{\gamma + \gamma_0}{|m_s|\omega^2}\left(\frac{k_{\mathrm{B}} T}{|m_s|} + \frac{v_i^2}{2}\right), \quad \textbf{[6]}$$

where $v_{\mathrm{i}}$ is the soliton's initial velocity. The offset $\gamma_0$ accounts for any diffusion present without impurities. The friction coefficient $\gamma$ is given by

$$\gamma = \frac{2\hbar}{k_{\mathrm{B}} T}\sum_{m,l}\int_{-\infty}^{\infty}\frac{dk_z}{2\pi}k_z^2\left|\frac{\partial\epsilon}{\partial k_z}\right| R(k_z)n(\epsilon)\left[1 + n(\epsilon)\right], \quad \textbf{[7]}$$

an extension of ref. 23. $\epsilon_{m,l}(k_z) = \hbar^2 k_z^2/2m_{\mathrm{Rb}} + \hbar^2 j_{m,l}^2/2m_{\mathrm{Rb}}R_\perp^2$ is the impurities' quasi-1D dispersion along with quantized states in the radial direction, described by Bessel functions. We account for radial confinement by summing over quantum numbers $m$ and $l$. $n(\epsilon)$ is the Bose–Einstein distribution for impurity atoms[‡].

Fig. 4*B* plots $D$ measured experimentally (markers) and computed theoretically (curves; colored for different temperatures) as a function of $N_I/N$. The theory provides rather accurate estimates of the experimentally observed diffusion coefficient, with a single fitting parameter given by $\gamma_0 = 5.32 \times 10^{-4}\ \mathrm{mm}^2/\mathrm{s}$. $\gamma_0$ is set by the diffusion coefficient at $N_I/N = 0$, where $D$ is suppressed in agreement with our theory. Diffusion at zero impurity concentration could be due to a number of factors, including scattering of thermal phonons from the soliton, as well as trap anharmonicity (6, 16). In our quasi-1D system, the soliton is not reflectionless to phonons in the majority gas as it would be in 1D.

## Conclusion and Outlook

Our data show that added uncondensed impurity atoms contribute to soliton diffusion; however, the soliton lifetime falls monotonically with increasing impurity fraction, even when the additional impurities all enter the condensate. We speculate that this might arise from two independent effects: (*i*) A static soliton forms a potential minimum for impurity atoms, implying that, after some time, impurities will congregate in these

[‡]In our model, the condensed atoms do not contribute to the stochastic force underlying diffusion because they are all in the ground state. The impurity atoms are condensed for impurity fraction $\gtrsim 0.2\%$; thus, the number of thermal impurity atoms is constant, leading to constant friction coefficient.

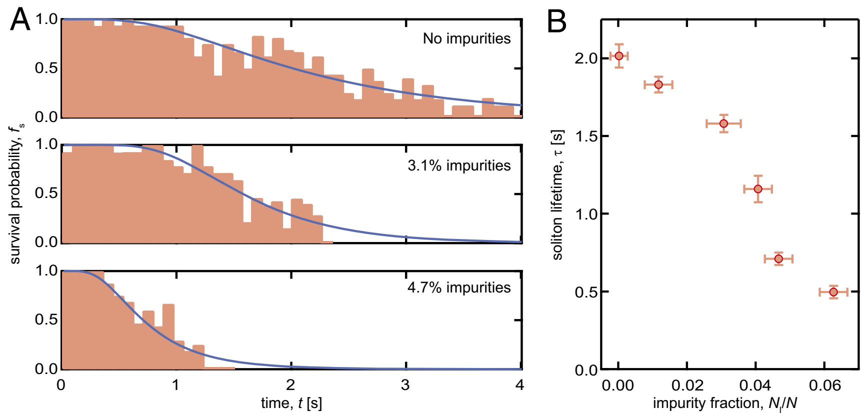


**Fig. 3.** Soliton lifetime in the presence of impurities. (*A*) Histograms of soliton occurrence probability $f_s$ vs. time $t$ after phase imprint. The blue solid curves are fits to the lognormal-based survival function, from which we extract the lifetime $\tau$. For each impurity fraction, we stopped collecting data when $f_s$ fell below approximately 0.2. (*B*) Lifetime $\tau$ extracted from fit to the survival fraction $f_s$ vs. impurity fraction $N_I/N$.

minima (7), broadening and destabilizing the soliton; or (*ii*) because the soliton moves in excess of the speed of sound for the impurity atoms, even condensed atoms can reflect from the moving soliton. Although this coherent reflection process would not add to diffusion, it would transfer momentum, thereby increasing the apparent damping coefficient and thereby reducing the soliton lifetime. This latter model predicts a reduction of lifetime qualitatively similar to, but quantitatively in excess of, that observed in experiments.

Solitons in spinor systems with impurity scatterers is an exciting playground for studying integrability breaking and diffusion of quasiclassical, negative-mass objects. Our observed reduction in soliton lifetime with increasing impurity fraction is in need of a quantitative theory. For the case of no impurities, there is a further open question for both theory and experiment of whether friction and diffusion can be present, even in the case of preserved integrability, for example, due to non-Markovian effects, as was recently discovered for bright solitons (24). Future experiments could study the impact of different types of impurities on soliton dynamics by introducing impurities of a different atomic mass. Lastly, mixtures with tunable interactions could freely tune the amount of impurity scattering, offering an additional way to change $D$.

## Materials and Methods

**BEC Creation.** We created BECs in the optical potential formed by a pair of crossed horizontal laser beams of wavelength $\lambda = 1064$ nm (11). The beam traveling orthogonal to the elongated direction of the BEC was spatially dithered by modulating the frequency of an acoustic-optic modulator at a few hundred kHz. This created an anharmonic, time-averaged potential. To reach the extremely cold temperatures necessary to realize long-lived solitons, we evaporated to the lowest dipole trap depth in which our technical stability allowed us to realize uniform BECs.

**Temperature Measurement.** We measured temperature below the majority atom's condensation temperature $T_c = 350$ nK by removing the majority atoms and fitting the TOF expanded impurity atoms to a Maxwell–Boltzmann (MB) distribution (13). Once the temperature was below $T_c$ for the impurity atoms, MB fits systematically underestimated the temperature. Fitting the small number of impurity atoms to a Bose distribution was technically challenging due to low signal-to-noise ratio and the addition of another free parameter, the chemical potential. To limit the number of free parameters, we performed a global fit on the different impurity fractions, where we constrained the chemical potential $\mu$ to be negative. This provided an estimate of the temperature with large uncertainties. We found for our usual operating parameters, and, based on information from both temperature measurements, $T = 10(5)$ nK.

**Impurity Characterization.** We used a Blackman enveloped rf pulse at a $\sim$ 9 G magnetic field to transfer the $|F = 1, m_F = 0\rangle$ atoms primarily to the $|F = 1, m_F = +1\rangle$ internal state (25). We varied the impurity fraction by tuning the rf amplitude. Even though the fraction of impurity atoms before evaporation determined the fraction after evaporation, they were not equal due to more effective evaporation of the minority spin state (13). We characterized the impurity fraction through careful, calibrated absorption imaging with a Stern–Gerlach technique during TOF to measure the relative fraction of the impurity atoms after evaporation.

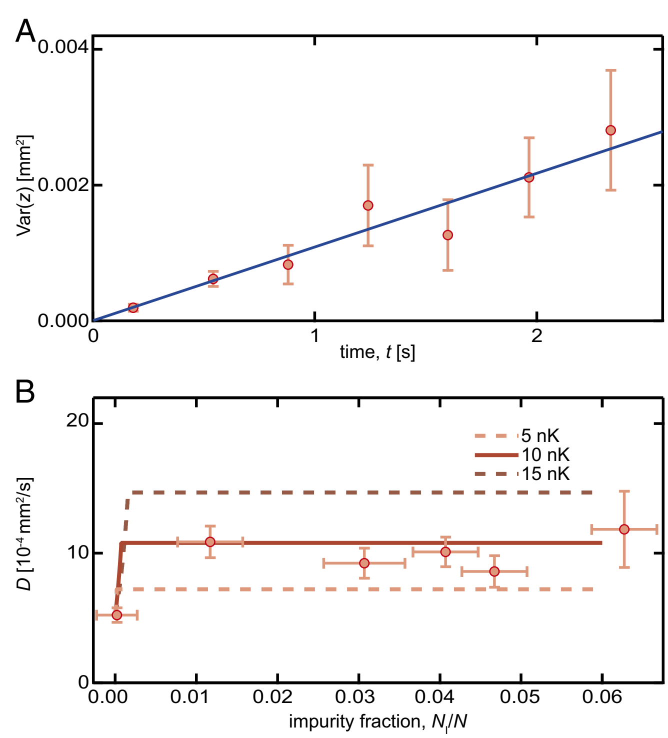


**Fig. 4.** Brownian diffusion constant dependence on impurities. (*A*) An example for the linear fit of Var($z$) vs. $t$ for 1.2% impurities. Data are binned into 0.36-s bins; the uncertainties are the sample SD. (*B*) The diffusion coefficient $D$ vs. impurity fraction $N_I/N$. The experimental results (markers) are extracted from the slope of a linear fit of the sample variance Var($z$) vs. time $t$. The uncertainty in $D$ is the uncertainty from that fit. See Materials and Methods for an explanation of uncertainty in $N_I/N$. The theory curves (solid and dashed curves) plot the calculated $D$ for our measured temperature.

**Soliton Creation.** We applied a phase shift to half of a condensate by imaging a back-lit, carefully focused razor edge with light red detuned by $\approx 6.8$ GHz from the $D_2$ transition for 20 μs.

**Scattering Theory of Impurities.** Minimizing Eq. **4** with respect to $\varphi^*$, $\psi^*$ gives the coupled equations of motion

$$i\hbar\partial_t\varphi(z,t) = -\frac{\hbar^2}{2m_{\mathrm{Rb}}}\partial_z^2\varphi(z,t) + g|\varphi|^2\varphi + \frac{g'}{2}|\psi|^2\varphi, \qquad [8]$$

$$i\hbar\partial_t\psi(z,t) = -\frac{\hbar^2}{2m_{\mathrm{Rb}}}\partial_z^2\psi(z,t) + \frac{g'}{2}|\varphi|^2\psi. \qquad [9]$$

In the experiment, we observed that the soliton remained stable for long times in the presence of impurities. Therefore, we neglect the last term of Eq. **8**, giving the well-known solitonic solution in Eq. **1**. We seek a solution for the impurity wavefunction $\psi(z)$ in the soliton rest frame. In the radial direction, the single-particle wave functions are the usual Bessel functions for a particle in a cylindrical well. For $\psi(z)$, we combine Eqs. **1** and **9** with $\psi(z,t) = e^{-iE_z t/\hbar}e^{im_{\mathrm{Rb}}v_s z'/\hbar}\psi(z')$. This gives a Schrödinger equation with a Pöschl–Teller potential (18, 20),

$$\frac{\partial^2\psi(z')}{\partial z'^2} + \left[\frac{\gamma_s^2\lambda(\lambda-1)}{\cosh^2(\gamma_s z')} + k_z^2\right]\psi(z') = 0. \qquad [10]$$

The dimensionless parameters are $z' = (z - v_s t)/\sqrt{2}\xi$, $k_z^2 = 4m_{\mathrm{Rb}}\xi^2/\hbar^2\left(E_z + m_{\mathrm{Rb}}v_s^2/2 - g'\rho_0/2\right)$, $\lambda(\lambda-1) = 2m_{\mathrm{Rb}}\xi^2 g'\rho_0/\hbar^2 = g'/g$, and $\gamma_s = \sqrt{1-(v_s/c)^2}$. $g$ and $g'$ are the effective 1D interaction parameters after integrating over the transverse degrees of freedom in $\psi$ and $\varphi$. Because the transverse wave functions are different, in general, $g'/g \lesssim 1$. However, $R(k_z)$ is periodic in $g'/g$ (through $\lambda$), and small variations in this parameter do not strongly affect the result. Solving for $\psi(z')$ and the scattering matrix then gives $R(k_z)$ Eq. **5**. For $\lambda \approx 1.5$, this potential also has a single, shallow bound state. Occupation of the bound state by an impurity atom can only occur through three body collisions (two impurity atoms and soliton), scenarios that we did not consider here.

**Kinetic Theory of the Soliton.** To define a diffusion coefficient, we studied the distribution function of many solitons, $f(t, z(t), v_s(t))$ (corresponding to many experimental runs). The distribution function of solitons follows a Boltzmann equation with a collision integral in Fokker–Planck form

$$\frac{df}{dt} = \frac{\partial}{\partial p}\left(Af + B\frac{\partial f}{\partial p}\right), \qquad [11]$$

where $A$ and $B$ are the drift and diffusion transport coefficients, and the left-hand side is a total time derivative. For $v_s \ll c$, we can write $A \approx \gamma v_s$ and $B \approx \gamma k_B T$, where $v_s$ is the soliton velocity and $\gamma$ is the friction coefficient given in Eq. **7**. Finally, we write the soliton momentum as $p = -|m_s|v_s$ (23). The kinetic equation then takes the form

$$\frac{\partial f}{\partial t} + v_s\frac{\partial f}{\partial z} = \frac{\partial}{\partial v_s}\left(-\Gamma v_s f - \frac{\partial_z V}{|m_s|}f + \Gamma v_{th}^2\frac{\partial f}{\partial v_s}\right), \qquad [12]$$

where $\Gamma = \gamma/|m_s|$ and $v_{\mathrm{th}}^2 = k_B T/|m_s|$ is the thermal velocity. This equation can be solved analytically by using the method of characteristics in the case of a harmonic potential $V(z) = -|m_s|\omega^2 z^2/2$. The solution is the time-dependent distribution function $f(t, z, v_s)$, parametrized by functions $g_i(t,\omega)$, with Gaussian form

$$f(t,z,v_s) = \frac{1}{2\pi\sqrt{4g_1g_3 - g_2^2}}\exp\left\{-\frac{1}{4g_1g_3 - g_2^2}\left[g_1v_s^2 + g_3z^2 + g_2v_sz + v_iv_s(g_2g_4 + 2g_1g_5) + v_iz(g_2g_5 + 2g_3g_4) + v_i^2(g_3g_4^2 + g_1g_5^2 + g_2g_4g_5)\right]\right\}. \qquad [13]$$

where $v_i$ is the soliton initial velocity and functions $g_i(t,\omega)$ are given by

$$g_1(t,\omega) = \frac{1 + 4\omega^2(e^t - 1) - e^t\left[\cos(t\bar\omega) + \bar\omega\sin(t\bar\omega)\right]}{2\omega^2\bar\omega^2} \qquad [14]$$

$$g_2(t,\omega) = -\frac{2e^t}{\bar\omega^2}\left[1 - \cos(t\bar\omega)\right] \qquad [15]$$

$$g_3(t,\omega) = \frac{1 + 4\omega^2(e^t - 1) + e^t\left[\bar\omega\sin(t\bar\omega) - \cos(t\bar\omega)\right]}{2\bar\omega^2} \qquad [16]$$

$$g_4(t,\omega) = -\frac{2e^{t/2}}{\bar\omega}\sin\left(\frac{t\bar\omega}{2}\right) \qquad [17]$$

$$g_5(t,\omega) = -\frac{e^{t/2}}{\bar\omega}\left[\sin\left(\frac{t\bar\omega}{2}\right) + \bar\omega\cos\left(\frac{t\bar\omega}{2}\right)\right], \qquad [18]$$

where we work in dimensionless units $t \to t/\Gamma$, $\omega \to \omega\Gamma$, $v_s \to v_{\mathrm{th}}v_s$, $z \to v_{\mathrm{th}}z/\Gamma$, and $\bar\omega = \sqrt{4\omega^2 - 1}$. Eq. **12** does not have a stable solution where $\partial f/\partial t \to 0$, due to the fact that the soliton is inherently unstable. The solution given in Eq. **13** is valid for $v_s \ll c$. Finally, we calculate the variance in soliton position, $\mathrm{Var}(z)(t) = \int dv_s \int dz\, z^2 f(t,z,v_s) = 2g_1 + v_i^2 g_4^2$, finding the exact expression (with restored units)

$$\mathrm{Var}(z)(t) = \frac{4v_{\mathrm{th}}^2(e^{\Gamma t} - 1)}{4\omega^2 - \Gamma^2} + \frac{4v_i^2 e^{\Gamma t}}{4\omega^2 - \Gamma^2}\sin^2\left(\frac{t\bar\omega}{2}\right) + \frac{v_{\mathrm{th}}^2\Gamma^2 e^{\Gamma t}}{\omega^2(4\omega^2 - \Gamma^2)}\left[1 - e^{\Gamma t}\left(\cos(t\bar\omega) + \frac{\bar\omega}{\Gamma}\sin(t\bar\omega)\right)\right] \qquad [19]$$

where $\bar\omega = \sqrt{4\omega^2 - \Gamma^2}$. In the limits $\Gamma t \ll 1$, $\Gamma \ll \omega$, we find diffusive behavior $\mathrm{Var}(z) \approx D(t)t$, with the time-dependent diffusion coefficient

$$D(t) \approx \frac{v_{\mathrm{th}}^2\Gamma}{\omega^2} + \frac{v_i^2\Gamma}{\omega^2}\sin^2\left(\frac{t\bar\omega}{2}\right). \qquad [20]$$

Setting $\sin^2(t\bar\omega/2) \approx 1/2$, we find the diffusion coefficient $D$ presented in Eq. **6**. We note that in the limit $\Gamma t \ll 1$, $\omega \to 0$, we have $\mathrm{Var}(z) \propto \Gamma t^3$—the variance has no linear in $t$ dependence, and the soliton undergoes ballistic motion, followed by exponential increase of $\mathrm{Var}(z)$ and soliton death§.

**ACKNOWLEDGMENTS.** We thank Martin Link and Stephen Eckel for carefully reading our manuscript; and Joachim Brand for greatly beneficial conversations. This work was partially supported by the Army Research Office's Atomtronics Multidisciplinary University Research Initiative, by the Air Force Office of Scientific Research's Quantum Matter Multidisciplinary University Research Initiative, National Institute of Standards and Technology, and the National Science Foundation through the Physics Frontier Center at the Joint Quantum Institute. H.M.H. received additional fellowship support from the National Physical Science Consortium and National Security Agency. V.M.G. was supported by the Simons Foundation.

§Our trap was not strictly harmonic; however, the restoring force emerges for any trap with nonzero slope $\partial_z V \neq 0$, making our results qualitatively applicable to our experimental set.

1. Strecker KE, Partridge GB, Truscott AG, Hulet RG (2002) Formation and propagation of matter-wave soliton trains. *Nature* 417(6885):150–153.
2. Khaykovich L, et al. (2002) Formation of a matter-wave bright soliton. *Science* 296(5571):1290–1293.
3. Burger S, Bongs K, Dettmer S, Ertmer W, Sengstock K (1999) Dark solitons in Bose-Einstein condensates. *Phys Rev Lett* 83(25):5198–5201.
4. Denschlag J, et al. (2000) Generating solitons by phase engineering of a Bose-Einstein condensate. *Science* 287(5450):97–101.
5. Ku MJH, et al. (2014) Motion of a solitonic vortex in the BEC-BCS crossover. *Phys Rev Lett* 113(6):065301.
6. Muryshev A, Shlyapnikov GV, Ertmer W, Sengstock K, Lewenstein M (2002) Dynamics of dark solitons in elongated Bose-Einstein condensates. *Phys Rev Lett* 89(11):110401.
7. Becker C, et al. (2008) Oscillations and interactions of dark and dark-bright solitons in Bose-Einstein condensates. *Nat Phys* 4(6):496–501.
8. Weller A, et al. (2008) Experimental observation of oscillating and interacting matter wave dark solitons. *Phys Rev Lett* 101(13):130401.
9. Hasegawa A, Matsumoto M (2003) Optical Solitons in Fibers, eds Kamiya T, Venghaus H, Monemar B, Yamamoto Y (Springer, Heidelberg), 3rd Ed, Vol 2, p 205.
10. Anderson BP, et al. (2001) Watching dark solitons decay into vortex rings in a Bose-Einstein condensate. *Phys Rev Lett* 86(14):2926–2929.
11. Lin Y-J, Perry AR, Compton RL, Spielman IB, Porto JV (2009) Rapid production of $^{87}$Rb Bose-Einstein condensates in a combined magnetic and optical potential. *Phys Rev A* 79(6):063631.
12. Fang F, Olf R, Wu S, Kadau H, Stamper-Kurn DM (2016) Condensing magnons in a degenerate ferromagnetic spinor Bose gas. *Phys Rev Lett* 116:095301.
13. Olf R, Fang F, Marti GE, MacRae A, Stamper-Kurn DM (2015) Thermometry and cooling of a Bose-Einstein condensate to 0.02 times the critical temperature. *Nat Phys* 11:06196.

14. Mateo AM, Brand J (2015) Stability and dispersion relations of three-dimensional solitary waves in trapped Bose-Einstein condensates. *New J Phys* 17(12):125013.
15. Zaremba E (1998) Sound propagation in a cylindrical Bose-condensed gas. *Phys Rev A* 57(1):518–521.
16. Parker NG, Proukakis NP, Adams CS (2010) Dark soliton decay due to trap anharmonicity in atomic Bose-Einstein condensates. *Phys Rev A* 81(3):033606.
17. Cockburn SP, et al. (2011) Fluctuating and dissipative dynamics of dark solitons in quasicondensates. *Phys Rev A* 84(4):43640.
18. Pöschl G, Teller E (1933) Bemerkungen zur Quantenmechanik des anharmonischen Oszillators. *Z Phys* 83(3):143–151.
19. Cooper F, Khare A, Sukhatme U (1995) Supersymmetry and quantum mechanics. *Phys Rep* 251(5-6):267–385.
20. Cevik D, Gadella M, Kuru S, Negro J (2016) Resonances and antibound states of Pöschl-Teller potential: Ladder operators and SUSY partners. *Phys Lett A* 380(18-19):1600–1609.
21. Lifschitz E, Pitaevskii L (1981) *Physical Kinetics* (Butterworth-Heinemann, Oxford).
22. Konotop VV, Pitaevskii L (2004) Landau dynamics of a grey soliton in a trapped condensate. *Phys Rev Lett* 93(24):240403.
23. Fedichev PO, Muryshev AE, Shlyapnikov GV (1999) Dissipative dynamics of a kink state in a Bose-condensed gas. *Phys Rev A* 60(4):3220–3224.
24. Efimkin DK, Hofmann J, Galitski V (2016) Non-Markovian quantum friction of bright solitons in superfluids. *Phys Rev Lett* 116:225301.
25. Jiménez-García K, et al. (2010) Phases of a two-dimensional bose gas in an optical lattice. *Phys Rev Lett* 105(11):110401.